Mem. S.A.It. Vol. 93, 150

Memorie della

A search for Extreme Energy Cosmic Rays and nuclearites in TUS observations and a study of the relative exposures

M. Aglietta[1], A. Anzalone[2], M. Battisti[3], M. Bertaina[3], F. Bisconti[3], R. Caruso[4], A. Castellina[1], A. Cellino[1], F. Fenu[1,3], S. Ferrarese[3], D. Gardiol[1], A. Golzio[3], E. Guido[3], F. Isgrò[5], M. Manfrin[3], K. Shinozaki[3], and G. Trinchero[1]

[1] Istituto Nazionale di Astrofisica – Osservatorio Astrofisico di Torino, Strada Osservatorio 20, I-10025 Pino Torinese, Italy
[2] Istituto Nazionale di Astrofisica – Istituto di Astrofisica Spaziale e Fisica Cosmica, Via U. La Malfa 153 I-90146 Palermo, Italy
[3] Università di Torino, Dipartimento di Fisica, Via P. Giuria 1, I-10125 Torino, Italy, e-mail: bertaina@to.infn.it
[4] Università di Catania, Dipartimento di Fisica e Astronomia, Via S. Sofia 64, I-95123 Catania, Italy
[5] Università di Napoli Federico II, Dipartimento di Ingegneria elettrica e delle Tecnologie dell'Informazione, Via Claudio 21, I-80125 Napoli, Italy

Received: 9 January 2022; Accepted: 25 May 2022

Abstract. TUS (Track Ultraviolet Setup) is the first orbital detector designed to check the possibility of recording Extreme-Energy Cosmic Rays (EECRs) events at E > 100 EeV by measuring the fluorescence signal of Extensive Air Showers (EAS) in the atmosphere. Funded by the Russian Space Agency ROSCOSMOS, TUS has operated as a part of the scientific payload of the Lomonosov satellite between April 2016 and November 2017. The collected data have been analyzed to search for EECRs and for possible strangelets (nuclearites) and determine their properties through comparison with simulated candidates obtained by means of the ESAF (EUSO Simulation and Analysis Framework) software. No clear candidate has been identified. A study of the aperture and exposure acquired by TUS in EECR and nuclearite modes has been conducted. This study is extremely important in view of the present and future space-based missions related to EECRs such as Mini-EUSO, K-EUSO and POEMMA.

Key words. Stars: abundances – Cosmic Rays: Extreme Energy Cosmic Rays – Cosmic Rays: Extensive Air Showers – Dark Matter: Nuclearites – Telescopes: TUS

1. Introduction

The cosmic ray spectrum extends over more than ten orders of magnitude reaching energies well beyond those reachable by means of accelerators. Above $5{\times}10^{19}$ eV, these particles are called Extreme Energy Cosmic Rays (EECRs) and their rate becomes as low as one

event per century per square kilometer (Aab et al. , 2020).

The still unknown EECR sources probably involve physical processes occurring in extreme extragalactic environments as very few known astrophysical objects can satisfy the requirements imposed by the observed spectrum, composition, and lack of strong anisotropies (Kotera & Olinto , 2011). In particular, the lack of anisotropies towards the Galactic plane implies an extragalactic origin for protons at $E>10^{18}$ eV and $E>Z\times10^{18}$ eV for nuclei with charge Z, based on the Pierre Auger Observatory (Auger) limits on the dipole anisotropy amplitude (Abraham et al. , 2007), and according to reasonable models of Galactic magnetic fields. At these extreme energies, the interaction of EECR protons or nuclei with the cosmic microwave background photons produces pions or dissociate nuclei. These processes are known as the Greisen-Zatsepin-Kuz'min (GZK) effect (Greisen, 1966; Zatsepin & Kuz'min , 1966). This effect changes the shape of the spectrum above 3×10^{19} eV and limits the possible distances of EECR sources to less than 100 Mpc from Earth, (the so-called GZK sphere). Since the distribution of matter within the GZK sphere is anisotropic, the possibility of observing detectable anisotropies in the sky at extreme energies can provide information on the nearest sources. Although extremely large, the covering area being 3000 km^2 in case of Auger (Abraham et al. , 2010) in the Southern Hemisphere and 700 km^2 for the Telescope Array (TA) (Abu-Zayyad et al. , 2012) in the Northern one, current ground-based observatories do not produce a statistics of events sufficient to unveil the EECR sources. The expected anisotropy of the signal has been elusive and no single source of EECRs has been unambiguously identified so far. The observed distribution of arrival directions shows no departure from isotropy below $\sim4\times10^{19}$eV. At EECR energies, Auger tests for anisotropies based on correlations with starburst galaxies and AGNs show a departure from isotropy of 4σ and 2.7σ respectively (Aab et al. , 2018). TA reported an excess above 5.7×10^{19}eV in a region of the sky spanning about 25°, centered on equatorial coordinates R.A.=144°, Decl.=40°, with 3.2σ significance (Kim et al. , 2021). These significances are not high enough to claim a discovery. The limit of the cosmic ray energy spectrum observed by TA seems to be more likely due to the GZK effect, whereas Auger results tend to be in better agreement with a limit in the acceleration of the sources. The path to solve this puzzle requires a large increase in statistics at EECR energies. To reach this goal, an upgrade of the Pierre Auger Observatory (Castellina et al. , 2019) and the TA×4 extension (Kido et al. , 2019) are currently going on. However, it is easier to collect these events from space, where the detector volume can by far exceed that of current ground-based experiments. This is the main goal of the K-EUSO (Casolino et al. , 2017) and POEMMA missions (Olinto et al. , 2021). TUS (Klimov et al. , 2017), and the recently launched Mini-EUSO (Bacholle et al. , 2021) offer the possibility to pave the way, with the purpose of proving the observation principle and understanding the challenges of such measurements from space. These studies are part of the global multi-messenger effort to unveil the most powerful cosmic accelerators using cosmic rays, photons of a wide range of energies from radio to gamma-rays, neutrinos (observed at high energies by IceCube (Aarsten et al. , 2013)), and gravitational waves (discovered by the LIGO detector (Abbott et al. , 2016)). The combined power of this approach will produce a great progress in both physics and astrophysics of acceleration and interactions at energies well beyond the reach of laboratories.

An even more relevant open question in cosmology and particle physics is the nature of dark matter. Macroscopic dark matter, generally called macros (Jacobs et al. , 2015), is a broad class of dark-matter candidates, that represents an alternative to conventional particle dark matter. Within this category, nuclearites are strange quark nuggets, with overall neutrality ensured by an electron cloud that surrounds the nuclearite core, forming a sort of atom. Nuclearites travelling with galactic velocities are protected by their surrounding electrons against direct interactions with the atoms they might hit. Therefore, they only lose energy in

elastic collisions with atoms in the medium. Two formalisms have been elaborated by (De Rujula et al. , 1984) and (Sidhu Singh et al. , 2019) to describe the intensity of the light emission in air. Recently, it has been pointed out by (Anchordoqui et al. , 2021) that for a reference mass of 1 g, there is a huge discrepancy, of about 14 orders of magnitude, between the macro luminosity predicted by the two formalisms. A search for nuclearites using fluorescence light by means of a space-based observatory was proposed by the JEM-EUSO collaboration (Adams et al. , 2015) showing the potential of such a technique. The observing strategy developed by TUS to detect a different kind of events, namely meteors, can be adequate to search for nuclearites and provide the first experimental results on the search of these elusive particles from space.

The paper is structured in the following way. Section 2 summarizes the key elements of the detector and it reports on the efforts that have been done to implement the TUS configuration into the simulation software adopted for the interpretation of the data. Sections 3 and 4 describe the search for EECRs and nuclearites, respectively, in the acquired data as well as a methodological study to estimate the exposure. Conclusions and perspectives are outlined in Section 5. The results presented in this paper are an extract of those summarized in (Barghini et al. , 2021) and represent the Italian contribution to the analysis of TUS data.

2. The TUS detector and the ESAF framework

The Lomonosov satellite was launched on April 28, 2016, on a polar sun-synchronous orbit with inclination of 97.3°, period of ∼94 min, and altitude about 500 km. The Track Ultraviolet Setup (TUS) was operated regularly till late November 2017, when the Lomonosov satellite faced some technical problems that did not allow transmitting experimental data to Earth.

The TUS detector consisted of two main parts (Klimov et al. , 2017): a parabolic mirror-concentrator of the Fresnel type and a square-shaped 256-pixel photodetector in the focal plane of the mirror. The mirror had an area of about 2 m^2 with a focal distance of 1.5 m. A pixel field of view (FoV) equals 10 mrad, which results in spatial resolution of 5 km, and the overall TUS FoV is approximately 80 km $\times$ 80 km at the sea level. Each pixel of the TUS photodetector is a Hamamatsu R1463 photomultiplier tube. Light guides with square entrance apertures (15 mm $\times$ 15 mm) and circular outputs are employed to fill uniformly the detector's FoV. Each pixel has a black blind 1 cm above the light guide to protect it from stray light. An UV filter of 13 mm diameter and 2.5 mm thickness is placed in front of each PMT. The pixels are grouped in 16 identical photodetector modules. Each cluster has its own digital data processing system for the first-level trigger, based on a Xilinx Field-Programmable Gate Array (FPGA), and a high voltage power supply, controlled by the FPGA. The central processor board gathers information from all modules, controls their operation, and implements the second-level trigger algorithm.

The TUS electronics could operate in four modes, intended for detecting various fast optical phenomena in the atmosphere at different time scales with different time sampling. The main mode was aimed at registering EECRs and had a time sampling of 0.8 μs. Slower modes had time sampling of 25.6 μs, 0.4 ms (for studying Transient Luminous Events such as elves, sprites, blue jets, gigantic jets, etc.). An even slower mode of 6.6 ms was dedicated to the detection of meteors and has been used to search for nuclearites. The four operational modes could not be run in parallel, therefore, the selected mode had to be fixed at the start of each run. Waveforms in each mode consisted of 256 time samples.

The trigger scheme, common to all four modes was structured in two steps to allow background rejection and the acceptance of EECRs. The Block of Information unit, which managed the data acquisition for all scientific devices on board the Lomonosov satellite, could accept data from TUS at most once in 53–60 seconds. This external constraint imposed a lower limit to the acquisition dead time of the TUS detector. This limitation had

a severe impact on part of the analyses that are discussed in the following. Namely, ground flasher lights could not be triggered more than once and clearly recognized as repetitive signals; the estimation of the exposure had to assume that the detector was always operational among triggers; during the 50–60 seconds of dead time, the detector shifted the position by ∼400 km. Therefore, when the trigger capability is restored, the FoV has totally changed and might not be representative anymore of the monitored conditions at the time of the last trigger. During an accident at the beginning of the mission, 20% of the PMTs were destroyed and sensitivities of the remaining PMTs changed in comparison with preflight measurements. A number of attempts of in-flight calibration have been performed but none of them is fully reliable yet. This introduces a large factor of uncertainty in estimates of the trigger threshold and the signal intensity. As a consequence, all respective estimates presented below remain approximate.

In order to perform a deeper analysis of trigger events in EECR mode a dedicated version of ESAF (EUSO Simulation and Analysis Framework) (Berat et al. , 2010), which includes a modeling of TUS optics and detector responses, has been developed. ESAF takes care of the simulation of all the relevant processes from the shower simulation until the event reconstruction. Both fluorescence and Cherenkov light (reflected and back-scattered) productions are modeled in ESAF. All the simulated photons are affected by Rayleigh scattering and ozone absorption. Optionally, clouds can be simulated as a constant layer of variable altitude thickness and optical depth. Non-uniform cloud coverage is also included in ESAF. Once the photons reach the detector, they are taken over by the optics module and the Focal Surface (FS) response is simulated.

For what concerns the detector, and in particular the optics, two approaches have been developed in parallel. The first one adopts a parametric simulation module that calculates analytically the position of a photon on the focal surface and adds a Gaussian spread around this position. This is intended to be a fast working tool to test the features of the different optics designs in an approximated way. It is used in the exposure study, where several thousands of Extensive Air Showers (EASs) are simulated. Second, a full ray-tracing code is used in the actual optics design. As an example, this was done in the nuclearite study. Once the photons reach the FS, they are transported through the filter and the optical adapter before reaching the photocathode. All the relevant effects including geometrical losses, inefficiencies of the adapter and of filters are taken into account. A parametrization of the photomultiplier response is included in the electronics part. Quantum efficiency, dependence on the incident angle of photon, collection efficiency and cross talk are also taken into account. The signal is then amplified by a parameterized gain and the resulting output current is collected and treated by the Front End Electronics module. More details about TUS implementation in ESAF can be found in (Fenu et al. , 2021). Fig. 1 shows an example of the light profile and shower track expected to be detected from a 10^{21} eV proton EAS with 60° zenith angle.

3. A search for EECRs and a study of TUS exposure

During its mission, TUS registered almost 80,000 events in EECR operation mode, with a few of them being sufficiently interesting to be more deeply scrutinized, as they passed basic selection criteria on temporal and spatial evolution of the signal on the FS as expected from ESAF simulations of EECR events. This lead to select almost 120 TUS events. These events have a characteristic light curve (integral signal of all triggered channels) with a pronounced maximum and full duration at half-maximum (FDHM) from 40 to 80 μs, which is quite consistent with the simulated detector response to the EAS fluorescence (see Fig. 1). However, the amplitude of these events corresponds to EECR energies well above 10^{20} eV, and, consequently, their number is two orders of magnitude higher than expectations taking into account the limited exposure of the TUS experiment. Moreover, the majority of EAS-like events were registered above continents

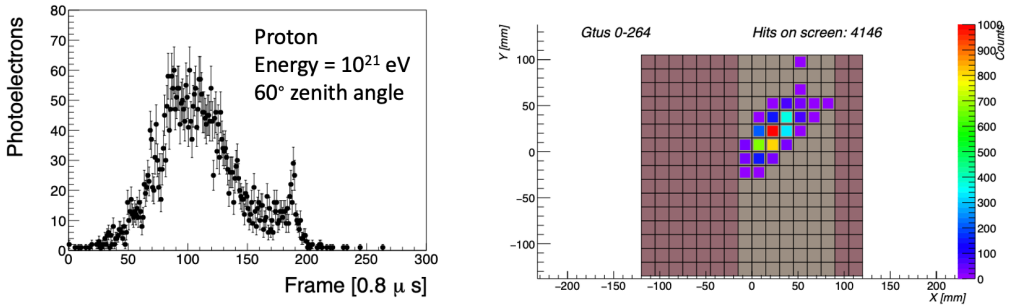

Fig. 1. A 10^{21} eV, 60° zenith angle simulated proton event. On the left: the photoelectron profile for the TUS detector; the bump at frame 190 is due to the Cherenkov reflection when the EAS reaches the ground. On the right: the photoelectron image for the TUS event. Image adapted from (Barghini et al. , 2021).

with half of them above the U.S., which immediately raises the question of their possible anthropogenic origin. Another feature of a simulated non-vertical EAS event is the presence of a noticeable movement of the signal along the photodetector matrix: the hit pixels are lined up along a rectilinear "track", and the displacement velocity is approximately proportional to $\tan(\theta/2)$, where θ is the zenith angle of the arrival direction. The aberrations of the TUS mirror lead to smearing of this track over neighboring pixels, which significantly complicates the determination of the motion. It turned out that only in 6 events the track length was sufficient to identify the movement of the image, reconstruct the track, and estimate the direction of arrival. They were registered above the U.S.. For five of them, airports were found in their close vicinity. A dedicated analysis showed that reconstructed arrival directions of all these events strongly correlate with directions of airport runways (Sharakin & Ruiz Hernandez , 2021). For the sixth one it was not possible to correlate the signal to the presence of an airport runaway. The event was located in Minnesota. A dedicated study of the weather conditions was applied (Khrenov et al. , 2020). The event occurred in perfect weather conditions. The map in Figure 2 shows that a series of low-pressure systems were developing on the central-western U.S. that was organised into a thunderstorm line proceeding from West to East and positioned above Dakota 18 hours later. However, there were no clouds

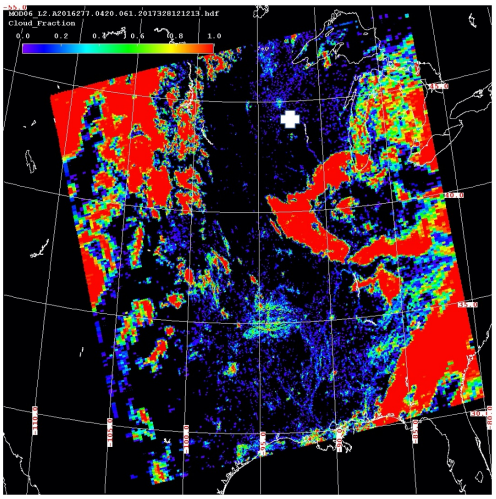

Fig. 2. MODIS cloud fraction at 4:20 UTC. Dark colour is clear sky while red colour indicate cloud fraction equal 1. The white cross shows the location of the TUS event.

on the eastern Minnesota and Wisconsin at 4:20 UTC, while fog was present in southern Wisconsin, which is depicted with red colours. Similar weather conditions emerged by looking at other satellite images, ground station reports and from atmospheric soundings. The peculiar detector response, the reconstructed kinematics and the energy assignment of this event above 10^{21} eV, if interpreted as an EECR, support the conclusion that also this event has a different origin than an EAS.

Despite the lack of successful EAS candidates, TUS data offer the opportunity to perform an estimation of the geometric exposure which is a much more complex topic than for ground-based experiments, as the atmopheric and illumination conditions are rapidly changing due to the satellite speed. The study reported in the following is based on events triggered in the EAS mode in the night segments of the Lomonosov orbits. The triggers are distributed quite uniformly with a higher concentration over continents. A notable exception to this is represented by Antarctica, the Arctic and Sahara, which remain quiet areas with the trigger densities comparable to those above the oceans. An estimate of the active time can be given for each orbit, under the assumption that the detector has always been in acquisition, except for the intrinsic dead time. 3118 orbits with a total acquisition time of 73 full days are identified. A total active time of 31 days is obtained as soon as the dead time is taken into account. This amounts to ∼42% of the total acquisition time. Such an estimate is based only on the identified orbits and could be potentially an underestimate of the real acquisition time. Thanks to the knowledge of the satellite trajectory, it was possible to estimate with a ∼1 second resolution the status of the detector for each position on the Earth map. Fig. 3 shows the active time fraction of the detector as a function of the geographical coordinate.

It can be seen that populated areas or stormy regions have very low active time basically not contributing to the cumulative exposure. Aurora ovals are also clearly visible as low active-time areas in the polar regions. On the other hand, oceans are very quiet areas, where EECR studies would be favoured. The presence of low or no-Moon illumination is verified in 21.2 full days of acquisition. The amount of active time in this condition amounts to 12.9 days, 60% of moonless acquisition time. The cloud condition for each trigger has been estimated based on (MERRA , 2021). It can be seen how most (∼ 70%) of the triggers are in cloudy conditions. It is therefore crucial to estimate the efficiency for EECR detection in presence of clouds. ESAF simulations are used for this, following the approach

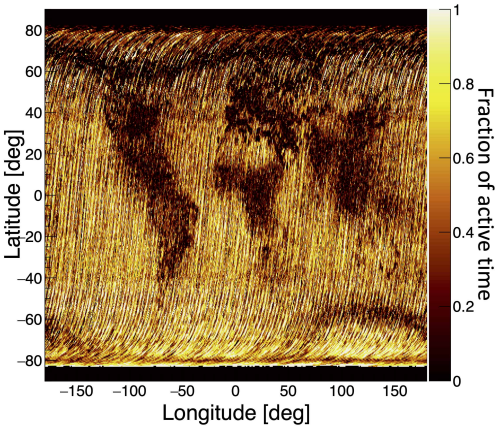

Fig. 3. Ratio of active time over the total amount of transit time as a function of geographical location. Image adapted from (Barghini et al. , 2021).

described in (Adams et al. , 2013). The signal recorded for each triggered event can be used to estimate the rate of photoelectrons generated by the airglow emission. Such information is used in the simulations to estimate the energy dependence of the exposure. In general, the rate of the background illumination varies from 1 to over 100 photoelectrons per frame unless rare cases such as above auroral ovals, night-day transitions, very populated areas, which anyway do not contribute significantly to the exposure as previously discussed.

The trigger performance is derived through Monte Carlo simulations. Two thousand EASs were injected in an area A_{simu} larger than the field of view (±150 km) to avoid border effects. Showers were simulated with zenith angles θ from 0° to 90° with a $\sin(2\theta)$ dependence and the azimuth from 0° to 360° uniformly. The TUS trigger logic was implemented in the ESAF simulation software and used for this estimation. Several trigger thresholds adopted in the mission were tested with an airglow rate of ∼18 photoelectrons per frame. The estimate of the trigger performance depends on a number of factors, among them the sensitivity of the photodetector, the level of the background illumination and software parameters of the trigger. As a result of taking into account the currently most accurate estimates based on the in-flight calibration, we obtain a trigger thresh-

old $\gtrsim$ 500 EeV. Moreover, the majority of the events could indeed trigger only above $\theta \approx 40°$–$50°$. This is a consequence of the trigger logic that rejects all events lasting for a short time, therefore, the most vertical ones.

Secondly, the efficiency of the trigger in cloudy conditions is simulated. One thousand EASs at fixed energy have been simulated for each cloud top height condition in a similar way as for clear sky. A higher cloud top height causes a significant reduction of the triggered events given the reduction of the amount of light reaching the detector. An estimate of the overall reduction of the exposure in the whole flight can be given by an average of the trigger efficiency weighted by the fraction of triggers in each condition. This leads to 57% of what is expected for the clear sky case. By taking into account the above factors, excluding the cloud impact, the geometrical exposure in clear sky conditions amounts to ~1550 km^2 sr yr. This value reduces to ~884 km^2 sr yr at $2 \cdot 10^{21}$ eV if the cloud impact is taken into account.

4. A search for nuclearites and a study of the TUS exposure

A search for nuclearites in the TUS data was performed assuming the (De Rujula et al. , 1984) model. Data were collected during about 250 h of nighttime observation in "meteor" mode, which has a sampling time of 6.55 ms. This analysis has to be considered as a methodological study in view of future space-based detectors. In fact, TUS was not developed with such an objective, therefore, the performance is not indicative of the full potential of a space-based telescope. However, it can provide a guidance and confirm the feasibility of the technique. The sensitivity is obtained under general assumptions that still need to be carefully assessed. A detailed description of the analysis on the search for nuclearites and on the estimation of the geometrical aperture is reported in (Shinozaki et al. , 2019).

The principle of the nuclearite search by TUS is based on the detection of a moving light spot in the atmosphere. A small modification is applied here to the original formula in (De Rujula et al. , 1984) to allow for arbitrary velocities (v), while originally this was assumed to be fixed at 250 km/s. The apparent brightness of the nuclearite expressed in stellar magnitude units $\mathcal{M}$ follows the relation:

$$\mathcal{M} = 10.8 - 1.67 \log_{10}(m/1\ \mu\text{g}) + 5 \log_{10}(r/10\ \text{km}) - 7.5 \log_{10}(v/250\ \text{km s}^{-1}), \quad (1)$$

where r is the distance to the observer and m the mass of the nuclearite. For simplicity, we also assume that the flux, defined for the V-band magnitude (λ = 550 nm) is constant over the wavelength range of TUS (250–400 nm). According to (De Rujula et al. , 1984), the maximum height where a nuclearite at v = 250 km/s can effectively generate the light, assuming a constant atmospheric scale height, is:

$$h_{\max} = 2.7\ \text{km} \cdot \ln(m/1.2 \cdot 10^{-5}\ \text{g}). \quad (2)$$

We used a realistic density profile function to convert the corresponding air density into height, which lowers $h_{\max}$. To search for nuclearites, TUS data were selected by requiring a nocturnal background level according to the high voltage level, the sub-satellite point at sea level at least 75 km away from the coast to minimize the effect of anthropogenic lights and the zenith angle of the Moon above 90° to eliminate direct moonlight on the focal surface of the detector. Moreover, only the good-quality PMTs, whose gain was estimated in flight to be of the order of 10^6, were considered.

In TUS, the main observables are the light curve and the angular velocity ω. In case of meteors, the light curve can drastically change in time due to ablation processes and fragmentation of the meteoroid, giving birth to even more than one luminosity peak. On the other hand, the intensity of the light spot from a nuclearite is expected to change only monotonously with the distance r. TUS can only measure the perpendicular component of the velocity $v_\perp$ seen from the observer, which is given by $r\omega$. The speed of the Sun relatively to that of the Galactic Center is usually considered to define the relative velocity of the nuclearites. However, by considering also the escape velocity from the Galaxy, an upper bound is set to the "relative" velocity in the frame of the observer at ~800 km/s. For this reason the

estimation of $\mathcal{M}$ takes into account also the velocity as a parameter. The definition of the aperture is done for three different cases: a) the standard one of 250 km/s, b) a lower bound at 75 km/s to be above the limit of the meteor speed, c) 800 km/s as an upper limit.

Since nuclearites may be seen as "fast" moving events, we looked for events in which the fastest peak channel was shifting faster than 0.13 rad/s, i.e. $v_\perp \geq 60$ km/s. After this selection, only 76 events remained, and on these we applied a visual inspection. None of the above candidates had a moving light spot compatible with simulations of nuclearite light tracks.

To interpret the data and to estimate the performance of the instrument, we carried out a full simulation study including radiation processes in atmosphere and detector response. To emulate the observation conditions, we checked the selection criteria along the orbit every 5 s by calculating the distance to the coast and Moon's zenith angle. To estimate the "on-time" T_0, we assumed that TUS was active for data taking in any 5-s segments if the elapsed time after the last trigger was longer than 53 s. The first event after TUS entered the Earth's umbra was excluded. By summing up these active segments, T_0 is estimated to be 47.4 hours. To include the presence of clouds that might reduce the observation area, we employed the MERRA2 dataset. It provides the global weather parameters outputs on 0.5°(latitude) × 0.625°(longitude)-grid points. The cloud-top height map is renewed every hour and the value is picked up every 5 s below the TUS position. To generate a simulated nuclearite event, we randomly sampled the conditions from all the active times to refer the cloud-top height to the TUS height and position. For an input mass of the nuclearite, the arrival direction and impact points are uniformly distributed onto a sphere with a radius R_0 beneath TUS. Among the generated $N_{\rm sim}$ events, the number $N_{\rm sel}$ that pass the event selection allows to compute the aperture as:

$$A_0 = 2\pi^2 R_0^2 \cdot (N_{\rm sel}/N_{\rm sim}). \quad (3)$$

The atmospheric model includes air and ozone densities to take into account wavelength-dependent Rayleigh scattering and ozone absorption. As a result, the maximum height of light emission by nuclearites is modified, from Eq. (2) and it is in general lower. Therefore, the effective volume of light emission in atmosphere decreases. As an example, at 1 kg mass the maximum height of light emission becomes ∼35 km to be compared with ∼50 km from the original formula. We generated the light from nuclearites only in the volume of atmosphere between the cloud-top-height and $h_{\rm max}$. We applied the ray trace and electronics response simulations with the background level and its fluctuation based on real data taken from the last TUS event at the sampled time. For all channels and ticks, the background is added with a Gaussian random generation. Simulation of nuclearite events was performed. To discriminate them from meteors and other moving events, it is important to have many channels with significant signals in order to determine the angular velocity and light curve properly. To estimate the sensitivity in terms of "aperture" of such an analysis, we applied relatively tight cuts on the simulated events. We required: a) ≥ 10 channels with the maximum counts above 25σ, and b) ≥ 10 ticks (∼ 66 ms) available to compute the motion analysis. Table 1 summarizes the results on the aperture A_0 for conditions a) and b), and the quality on the reconstruction of the angular velocity ω and orientation Ψ for b). Combinations of m = 0.1, 1 and 100 kg, and v = 75, 250, and 800 km/s were simulated.

To translate the geometrical aperture into an exposure, an estimation of the on-time T_0 and of the limiting magnitude $\mathcal{M}$ is needed. These two numbers are not straightforward. In particular, the 53–60 s off-time of the detector between events does not allow having an exact knowledge of the illumination conditions between two consecutive triggers, which prevents a precise assessment of the limiting magnitude $\mathcal{M}$ at each instant. Moreover, a calibration of the instrument is still in progress. Therefore, we derive the TUS sensitivity under the following best scenario, which is based on two assumptions that still require further investigation. We assume the capability of detecting masses above 100 g which corresponds to $\mathcal{M} < +6$ according to Eq. (1), which is com-

Table 1. Results of the estimated apertures A_0 for conditions a) and b) and of the quality of the angular velocity ω and orientation Ψ for b). Different combinations of v and m are simulated.

v [km s^{-1}]	a) A_0 [10^{14} cm^2 sr]			b) A_0 [10^{14} cm^2 sr]			$\sqrt{<(\Delta\omega/\omega)^2>}$			$\sqrt{<(\Delta\Psi)^2>}$		
m [g]	10^2	10^3	10^5	10^2	10^3	10^5	10^2	10^3	10^5	10^2	10^3	10^5
800	1.3	2.6	3.2	0.07	0.2	0.7	-	-	0.08	-	-	7.4°
250	0.3	0.9	2.0	0.1	0.6	1.5	0.08	0.29	0.33	14°	22°	30°
75	0.4	0.6	1.0	0.2	0.3	0.8	0.52	2.1	0.40	58°	39°	48°

pliant with the limits in meteor brightness (see (Barghini et al. , 2021) for details). Moreover, we assume $T_0 \sim 2$ day on-time, which implies that the detector was always functioning between consecutive triggers with weather conditions allowing the detection of nuclearites with the above limiting magnitude. Under these assumptions, the TUS limits remain 1-2 orders of magnitude above the galactic dark matter limit at any mass above 100 g (see (Barghini et al. , 2021) for further details on this estimation).

Despite the fact that the TUS sensitivity remains above the Galactic dark matter limit, it shows the potential of a space-based detector to provide comparable flux limits to other experiments, taking advantage of a large aperture. We underline that most of the limitations on the present result come from the fact that the instrument was not designed for this search, it was operated in "meteor" mode for only a short time, and an accident occurred at the beginning of the mission that reduced the detector performance. Despite those limits and constraints, the results support the findings by (Anchordoqui et al. , 2021; Abdellaoui et al. , 2017), which indicate that Mini-EUSO and POEMMA have the potential to cross the dark matter limit line.

5. Conclusions and perspectives

The TUS detector was the first space-based mission designed for EECR measurements. Its active operation lasted from May 2016 till November 2017. During the mission, several acquisition modes with different temporal resolution were tested to sense various physical phenomena, with the total geometrical exposure in the EAS mode reaching approximately 1550 km^2 sr yr. A number of events passing basic selection criteria on temporal and spatial evolution of the signal on the focal surface as expected from simulations of EECR with ESAF were carefully examined. None of them was clearly identified as EAS detections. This is due to the too high energy threshold of the detector (well above 10^{20} eV) which is partially due to the unfortunate accident that occurred at the beginning of the mission. Moreover, the TUS spatial resolution is inadequate to properly reconstruct the movement of the track in the FoV and the trigger system was fine-tuned for inclined EASs which reduced the effective aperture of the instrument. Strong limitations imposed by the data acquisition affected also significantly the effective measurement time of the instrument and the available exposure. It is important to underline here that such limitations have been overcome with Mini-EUSO on the International Space Station (ISS) and that future projects (K-EUSO and POEMMA) will have an order of magnitude higher spatial resolution and larger collecting power which will allow to reach detectability of EAS events well below 10^{20} eV.

A new version of the ESAF framework that includes the TUS detector was developed to assess the effective energy threshold of TUS, to scrutinize the events that passed the first selection criteria and to compute the geometrical aperture and exposure of the mission. The importance of associating all the above observations with an assessment of the weather con-

ditions was studied and the methodology was presented and applied to specific events.

The TUS detector registered various UV phenomena that constitute the background for EECR measurements. Among them are anthropogenic lights, thunderstorm activity and lightning discharges, upper atmosphere transient luminous events, polar lights, meteors and other phenomena, providing in some cases an imaging of these signals with an unprecedented sensitivity and time resolution. The capability of observing meteors allowed us to perform a methodological study and search for macroscopic dark matter events. TUS was not originally designed with this scientific motivation. In this regards, the results on nuclearites do not express the full potential of a space-based mission which relies on light emissions, however, it allowed to establish a methodology which can be repeated in future missions, starting with Mini-EUSO. A joint analysis of TUS and Mini-EUSO data will certainly help in further clarifying the origin of peculiar events that have been detected by TUS and whose origin has not been assessed yet.

In conclusion, we believe that TUS has demonstrated that the orbital fluorescent technique has a strong potential to measure and recognize a relativistic motion in the UV range in the atmosphere and to reconstruct the direction and energy of different events. On the other hand, the experience of the TUS mission reveals the difficulties of a space-based experiment that needs an accurate monitoring of the rapidly changing background illumination and a high-quality control of the sensitivity of the equipment. The TUS detector demonstrated a multi-functionality of an orbital fluorescent observatory and its usefulness for various astrophysical and geophysical studies. It provides an invaluable experience for the implementation of the future orbital missions like K-EUSO and POEMMA. The methods developed for the TUS data analysis are actively employed for studying and interpreting data of Mini-EUSO, which is currently operating at the ISS.

Acknowledgements. We highly appreciate the support of the Russian group and in particular of P. Klimov, S. Sharakin and M. Zotov for providing TUS data and for fruitful discussions during the analyses. Financial support from the agreement ASI-INAF n.2017-14-H.O is deeply acknowledged.

References

Aab, A., et al. 2018, ApJ, 853, L29
Aab, A., et al. 2020, Phys. Rev. D, 102, 062005
Aarsten, M. G., et al. 2013, Science, 342, 6161
Abbott, B. P., et al. 2016, Phys. Rev. Lett., 116, 061102
Abdellaoui, G., et al. 2017, Planet. Space Sci., 143, 245
Abraham, J., et al. 2007, Science, 318, 939
Abraham, J., et al. 2010, Nucl. Instr. Meth. A, 613, 29
Abu-Zayyad, T., et al. 2012, Nucl. Instr. Meth. A, 689, 87
Adams Jr., J., et al. 2013, Astrop. Phys., 44, 76
Adams Jr., J., et al. 2015, Exper. Astronomy, 40, 253
Anchordoqui, L A., et al. 2021, EPL Journal, 135, 51001
Bacholle, S., et al. 2021, ApJS, 253, 2
Barghini, D., et al. 2021, Advances in Space Res., doi:10.1016/j.asr.2021.11.044
Berat, C., et al. 2010, Astrop. Phys., 33, 221
Casolino, M., et al. 2017, PoS(ICRC2017), 368
Castellina, A., et al. 2019, arXiv:1905.04472
De Rujula, A., & Glashow, S. 1984, Nature, 312, 734
Fenu, F., et al. 2021, PoS(ICRC2021), 333
Greisen, K. 1966, Phys. Lett., 16, 148
Jacobs, D., et al. 2015, MNRAS, 450, 3418
Khrenov, B., et al. 2020, JCAP, 3, 033
Kido, E., et al. 2019, PoS(ICRC2019), 312
Kim, J., et al. 2021, PoS(ICRC2021), 328
Klimov, P., et al. 2017, Space Sci. Rev., 8, 1687
Kotera, K. & Olinto, A. V. 2011, ARA&A, 49, 119
MERRA: https://gmao.gsfc.nasa.gov/reanalysis/MERRA-2/
Olinto, A. V., et al. 2021, JCAP, 6, 007
Sharakin, S., & Ruiz Hernandez, O. 2021, JINST, 16, T07013
Shinozaki, K., et al. 2019, PoS(ICRC2019), 545
Sidhu Singh, J., et al. 2019, JCAP, 1902, 037
Zatsepin, G.T. & Kuz'min, V. A. 1966, JETP Lett., 4, 78